

Sample preparation and characterization steps towards Polariton Mediated Enhanced Conductivity

Hanne Roeland, s6899358

Master Program: Science and Business Management

Major Research Project, September 2019 - July 2020

Supervised by S.R.K. Rodriguez (Amolf Institute) and A.P. Mosk (Utrecht
University)

May 31st, 2022

Abstract

Recent experiments and calculations [1][2][3], suggest that the transport of charges can be strongly enhanced inside an optical cavity. This effect occurs when electronic excitations in a material are strongly coupled to a cavity mode. In this strong light-matter coupling regime, the hybridization between electronic and optical degrees of freedom redistributes the electronic density of states and opens new transport channels. The question stands: Can one modify the conductivity of a semi-conductor by strongly coupling electronic excitations in such semi-conductor to cavity modes. This thesis encompasses the preceding steps that had to be made in order to investigate whether and how the transport of charges can be strongly enhanced inside an optical cavity. For the purpose of this research 2(PEA) PbI_4 crystals were grown using the AVC method [4]. Platinum electrodes were made on top of DBRs using UV-lithography, E-beam evaporation, and chemical reactions in the lab. The crystals were exfoliated until right size and thickness and transferred onto the platinum electrodes. Lastly, the bare perovskite crystals were characterized both optically and electrically. The optical characterization shows an absorption peak at approximately $\lambda = 517nm$ and the PL shows a peak at approximately $\lambda = 527nm$. The electrical characterization was evaluated using the Simmons model. This thesis is a stepping stone for further research in polariton mediated enhanced conductivity in semiconductors.

Acknowledgements

I would like to express my gratitude to everyone who helped me write this thesis. First of all, my sincere gratitude for Said, for his endless patience and his help throughout the research. Many thanks to Zhou, for his daily supervision and for answering my many questions in the lab. Next, I'd like to thank Falco, Anne, Kevin, Johanna, Joris, Giel, Niels, and the rest of the Interacting Photons group for endless coffee breaks and fun (even as important as science). For technical support I would like to thank the cleanroom staff, Bob Krijger, Marc Duursma, and Niels Commandeur. Finally, I would like to thank the Nanoscale Solar Cells group and the Hybrid Solar Cells group for sharing their lab space with me and teaching me crystal chemistry.

Contents

1	Introduction	2
2	Background	4
2.1	Polaritons	4
2.2	Enhanced Charge Transport in Polariton Systems	7
3	Fabrication of Perovskite Semiconductor Crystals and Electrical Contacts	10
3.1	Perovskite Semiconductor Crystals	10
3.2	Electrical Contacts	13
4	Crystal Exfoliation and Transfer	21
4.1	Crystal Exfoliation	21
4.2	Deterministic Transfer onto Electrodes	24
5	Optical and Electrical Measurements	28
5.1	Optical Measurements	28
5.2	Electrical Measurement	30
6	Conclusion and Outlook	34

1 Introduction

This project is inspired by recent experiments and calculations [1][2][3], suggesting that the transport of charges can be strongly enhanced inside an optical cavity. This effect occurs when electronic excitations in a material are strongly coupled to a cavity mode. In this strong light-matter coupling regime, the hybridization between electronic and optical degrees of freedom can redistribute the electronic density of states and open new transport channels. In reference [3] the conductivity of organic semiconductors has even gone up 10 times.

The ultimate goal of this project is to insert a 2D perovskite semiconductor crystal into the cavity and to measure the conductivity as a function of cavity length. By varying the thickness of the perovskite and the cavity length the light-matter coupling strength and exciton-photon detuning can be controlled. The question stands: Can one modify the conductivity of a semi-conductor by strongly coupling electronic excitations in such semi-conductor to cavity modes.

Before inserting the perovskite into a microcavity and measuring its conductivity, some preceding steps had to be made:

- **Fabrication:** The perovskite semiconductor crystals that were used in this research had to be grown. To eventually measure the conductivity of these crystals, platinum electrodes were made on top of high reflectivity mirrors.
- **Exfoliation and Transfer:** The perovskite crystals had to be exfoliated until right size and thickness. After exfoliation they had to be transferred onto the platinum electrodes.
- **Optical and Electrical Characterization:** The bare perovskite crystals had to be characterised both optically and electrically.

This thesis encompasses the preceding steps that had to be made in order

to investigate whether and how the transport of charges can be strongly enhanced inside an optical cavity.

This thesis is structured according to the order of the steps mentioned above. Methods, results and discussion will be explained along the way following these steps.

2 Background

To understand whether and how the transport of charges can be strongly enhanced inside an optical cavity, some background is needed on polaritons and how these polaritons open up new charge transport channels.

2.1 Polaritons

The description of the interaction of light and matter can be explained at two levels, known as the weak and the strong coupling limits. In the weak coupling limit, the electromagnetic field of light and the excitations in matter are independent variables, they do not interact. In the strong coupling limit, there is an interaction between light (photons) and matter (QW excitons) and it is this interaction which leads to the formation of polaritons. A polariton is therefore a quasi-particle resulting from the strong coupling of an electromagnetic wave and an excitation in matter.

Excitons are the excited states in a semi-conducting crystal. They are the bound states of an electron in the conduction band and a hole in the valence band. Excitons can move freely within the crystal and transport energy, but not charge as they are electrically neutral. Excitons are unstable as the electron and the hole eventually will recombine. In semiconductors, excitons can be created either by the absorption of a photon having less energy than the bandgap but sufficient to excite an electron to an excitonic bound state, or by absorption of a photon having more energy than the direct bandgap which generates a free electron and a free hole which then relax in energy until they form a bound state.

In the semiconductor in this thesis, the excitons are weakly bound, making Wannier-Mott excitons. Wannier-Mott excitons are excitons where the attraction between the electron and the hole is small in comparison to the bandgap energy and their radius is much larger in comparison to the inter-atomic spacing. The binding energy of a typical semiconductor exciton is on

the order of 10 – 100 meV and its Bohr radius is about 10 – 100 Å, extending over tens of atomic sites in the crystal [5]. The electron and the hole form a dipole that interacts with the electromagnetic field of light. Its interaction strength varies with the excitonic oscillator strength.

A semiconductor quantum well is a thin layer of semi-conductor, sandwiched between two barrier layers with a much larger bandgap. If the material is thin enough (a thickness comparable to the Bohr radius of the exciton), quantum well excitons behave as two-dimensional quasi-particles. This confinement has several consequences. It modifies the valence band structure and the optical transition selection rules. Also due to the confinement, a quantum well exciton has a smaller Bohr radius and a larger binding energy compared to a bulk exciton, leading to an enhancement of the oscillator strength. This enhancement is often counteracted by a reduction in overlap between the light field and the exciton. So, to achieve a stronger exciton-photon coupling, it is necessary to also confine the photon field in the z-direction by introducing a microcavity.

A microcavity is typically a structure where a sample (in this case the semi-conducting perovskite) is sandwiched between two distributed Bragg reflectors (DBRs). A DBR is made of layers of alternating high and low refractive indices, each layer with an optical thickness of $\lambda/4$, where λ is defined as the wavelength. Light that reflects on each surface in the DBR destructively interferes with itself, creating a stopband (range of wavelengths) for transmission. So the DBR acts as a high-reflectance mirror whenever the wavelength of the incoming light is within the stopband. When the spacing between the mirrors is such that half a wavelength fits in the cavity, there will be a resonance in the cavity leading to a sharp increase in transmission. The photon field is then concentrated around the center of the cavity. This microcavity structure confines the light in the z-direction.

A cavity polariton is a quasiparticle resulting from the strong coupling between excitons and a strongly confined photon field in excitonic material.

Once the interaction energy between a photon and an exciton in a micro-cavity becomes sufficiently large, a back-transfer of energy becomes possible, the system is now in the strong coupling regime. It is no longer possible to distinguish between a donor and an acceptor. The excitation becomes delocalized and we must view the pair as one system [6]. So, the polariton is a linear superposition of an exciton and a photon. Since they are both bosons, so is a polariton.

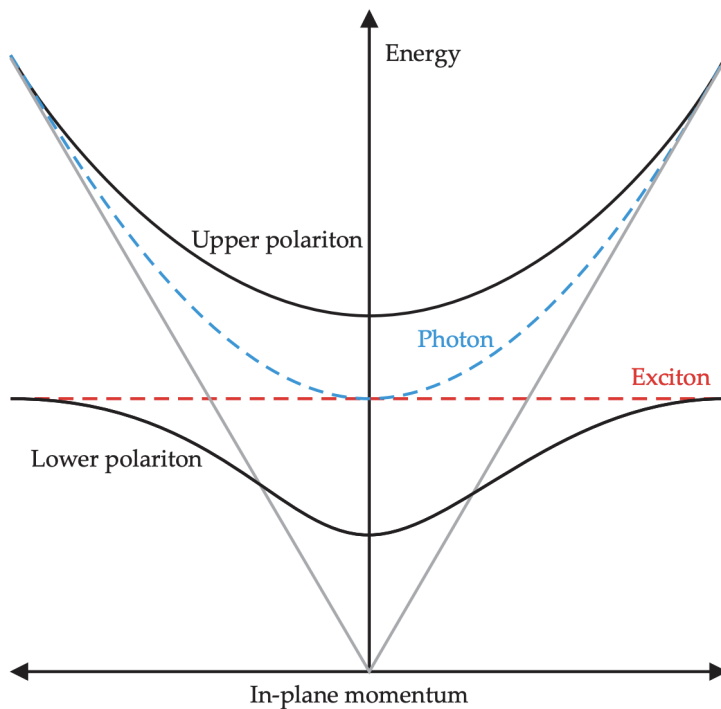


Figure 1: This schematic was taken from reference [7]. It shows the dispersion relation for a photon in an optical cavity. When the photon mode is tuned to the energy of an electronic excitation, exciton, photon-exciton coupling inside the cavity gives rise to new hybrid modes, polaritons (black lines).

Under the resulting strong coupling system, the dispersions anti-cross, as seen in figure 1 [7]. This anti-crossing results in two new dispersion relations for the upper polariton (UP, higher energy) and the lower polariton (LP, lower energy). The Rabi splitting of polaritons is the energy difference between the lower and the upper polariton at zero detuning and it is different

for the different materials that are used to create these exciton-polaritons. The exciton-polariton effective mass is predominantly determined by the photonic component, whose effective mass is much lighter and whose lifetime is much shorter than the excitonic part. The lifetime of the photons is determined by the quality of the DBRs (leakage of light from the cavity). The polariton lifetimes are determined by the photonic part and the polariton-polariton interactions are predominantly determined by their excitonic part. This results in extremely light quasiparticles with short lifetimes, but with a sizeable nonlinear interaction.

Particularly interesting for polariton physics are 2D hybrid organic - inorganic perovskites with large excitonic binding energies. The one used in this thesis: $2(C_6H_5C_2H_4NH_3)PbI_4$ or $2(Phenyl - Ethyl - Ammonium)Lead - Iodide$ or $2(PEA)PbI_4$ or PEPI crystals. This strong excitonic binding energy induces strong excitonic effects in these materials. The optical absorbance spectrum will have a sharp resonance, which is a consequence of dominating exciton transitions. The strong excitonic effects cause a significant oscillator strength from band-to-band transitions and this strong oscillator strength induces strong light-matter interactions [8]. Due to these characteristics, these perovskites make great candidates for exciton-polariton physics.

2.2 Enhanced Charge Transport in Polariton Systems

As stated in the introduction, this research was inspired by Orgiu et al.[3] “Conductivity in organic semiconductors hybridized with the vacuum field” [3]. In this article it is shown that the conductivity of an organic semiconductor can be enhanced by an order of magnitude. It shows an approach to improving carrier mobility: by injecting carriers into states that are hybridized to the vacuum field. To do so, organic semiconductors were strongly coupled to plasmonic modes to form coherent states that can extend over as many as 10^5 molecules and should therefore benefit conductivity [3]. The

current is then enhanced due to a change in field-effect mobility. The origin of the enhanced mobility can be explained by the extended coherence of the states induced by the hybridization with the vacuum field. This occurs over lengths that correspond to the mode volume, in contrast to the normal situation where the carrier is mostly confined to the molecular scale.

Large vacuum Rabi splittings have been reported for strongly coupled molecules, which significantly modifies the electronic structure of the molecular material. Organic semiconductors are of great interest in conducting devices due to their potential in making large, flexible and inexpensive materials. They are, however, limited by their charge carrier mobility due to disorder in these materials. In theory, charge carrier mobility should be enhanced by the extended coherence associated with light-matter coupling. Disorder in semiconductors in one dimension is known to lead to wavefunction localization and thereby vanishing conductivity. When coupling this system to the vacuum electromagnetic field it is expected that polaritonic states delocalized throughout the mode volume should appear [3]. The electronic component of the polaritonic state is delocalized despite the disorder in this strong coupling regime. In addition to the polaritonic state it is found that under strong coupling conditions, other electronic states in the conduction band are also modified by the hybridization with the vacuum field and become delocalized. These circumstances affect the conductivity positively.

In Orgiu et al.[3], “Conductivity in organic semiconductors hybridized with the vacuum field”, several materials with intense absorption bands are used to strongly couple to surface plasmon resonances. The conductivity of strongly coupled organic semiconductors to plasmonic modes is compared to the conductivity of the bare molecular material. This is done by recording IV-curves for both cases for thin films on top of a hole array between 2 electrodes. As a result, peaks in the current are visible when plotted against in-plane momentum. These current peaks correspond directly to the intersections of the molecular absorption and the surface plasmon modes. So,

current is boosted when an organic semiconductor is strongly hybridized with the surface plasmon modes. The current can be enhanced by an order of magnitude in this strongly coupled regime.

Orgiu et al. have shown that it is possible to enhance conductivity in some materials under strong coupling. Since this paper has been published, several research groups have tried to replicate their research with no success [9] [10]. The scope of this research is to find out whether there is the possibility to enhance a materials conductivity under strong light-matter coupling.

3 Fabrication of Perovskite Semiconductor Crystals and Electrical Contacts

For the purpose of this research $2(PEA)PbI_4$ (Phenyl-Ethyl-Ammonium Lead-Iodide) perovskite crystals were grown in the lab. These particular perovskite crystals are chosen for several reasons:

- technological relevance and potential (solar cells, perovskite detectors, etc.)
- availability and interest at the host research institute, Amolf
- high reflectance mirrors with a maximum reflection at $\lambda = 530nm$ are used for measurements and these crystals have photoluminescence and absorption peaks close to this value

To measure the conductivity of these crystals, platinum electrodes were made on top of distributed Bragg reflectors (high reflectance mirrors). In this chapter, the process of making semiconductor perovskite crystals and electrical contacts is explained.

3.1 Perovskite Semiconductor Crystals

Hybrid organic-inorganic perovskites have shown to be advantageous for optoelectronic applications. One key aspect that was made use of in this thesis is the ability to synthesize large areas of mono-crystalline thin films. For this specific research 2D Phenyl-Ethyl-Ammonium Lead iodide ($2(PEA) PbI_4$) crystals were synthesized using the “Anti-solvent Vapor-assisted Crystallization” (AVC) method [4]. These crystals are very well suitable for optoelectronic devices working with cavity-polariton quasi-particles [11] [12]. To make these crystals suitable, large grains of mono-crystalline thin films are needed. The thickness is controlled by a seemingly simple process called “the scotch tape method”, this will be discussed in a later chapter.

To start the synthesis of the crystals a precursor has to be made. A precursor is a solution which contains all the necessary components for the crystal structure, solved in a preferred type of solvent. This precursor is made to have a 1M concentration. For a 1M precursor solution, 2,305 g PbI_2 and 2,480 g PEAI are dissolved in their solvent, 5 mL of γ -butyrolactone (GBL). This mixture is then heated at 50 °C until complete dissolution.

Once the precursor is finished, a set-up has to be made. The set-up has to be left alone for five days minimum. A cartoon of the set-up can be seen in figure 2. 2 mL of precursor is put into a small vial. This small vial is left open and put into a larger vial which must be able to be sealed with a cork so the set-up is airtight. Inside the large vial, antisolvent is placed. This antisolvent is dichloromethane (DCM). This set-up is sealed with a cork and left alone for 5 days minimum.

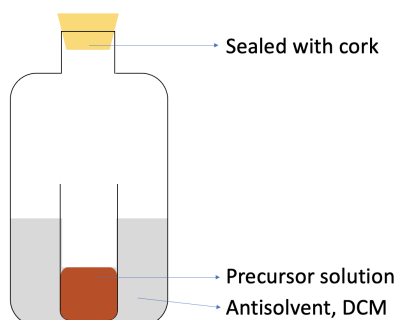


Figure 2: Cartoon of the set-up. A smaller vial with precursor solution is put into a larger vial sealed with a cork. This larger vial should be sealed so that it is airtight.

The anti-solvent will diffuse into the precursor solution and decrease its solubility. The effect of this decreased solubility is that the molecules in the precursor will recombine and form crystals. Crystallization is a very sensitive process and for the formation of big mono-crystalline crystal surfaces the crystallization should happen in a controlled environment. An ideal crystallization process takes place in a very cold environment with no vibrations. Since this was not achievable at the Amolf facilities, the set-up was placed

in a wet-bench in a relatively quiet place. For even larger crystals with less imperfections, there is room for improvement.

After 5 days, the set-up will look like in figure 3. As can be seen in the figure, the DCM has completely diffused into the precursor solution. Dark orange crystals can be seen on the inside of the smaller vial. These are the $2(\text{PEA})\text{PbI}_4$ crystals. These crystals can now be taken out of the solution and dried under a warm lamp. In figure 4 a photo of the crystals after drying can be seen. These 3D crystals can reach a lateral size of approximately 1 cm, which is quite large for single-crystal perovskites. When left in solution for more than 5 days, the crystals are able to grow even bigger.



Figure 3: The set-up after a crystallization period of five days. The antisolvent has diffused into the smaller vial and dark-orange crystals have formed inside the small vial.

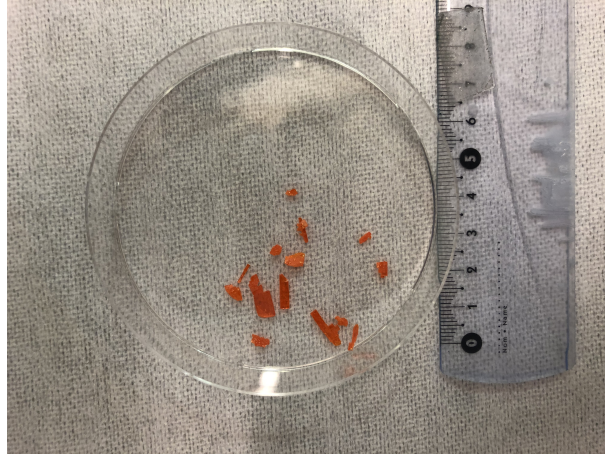


Figure 4: The crystals after drying beneath a warm lamp. Some reach a lateral length of 1cm.

3.2 Electrical Contacts

In this paragraph, the process of making electrodes on a DBR mirror is explained. To facilitate the measurement of the conductivity of the crystals inside a microcavity, platinum contacts were made on top of a high-reflectivity DBR mirror. This structure (DBR mirror with attached electrodes) makes one half of the microcavity that is used in the experiment. The DBR mirror has a glass surface on top of which these contacts are made. The contacts consist of a pattern of platinum electrodes, a picture of which can be seen in figure 5. On the left side of figure 5, 5 mm long platinum "fingers", from left to right, can be seen. Each platinum finger is numbered with an even number from 1 to 100, so there are 50 fingers. On the right side of this figure is a large slab of platinum. The fingers on the left and the slab of platinum are separated by approximately 2 microns, see figure 6 for a microscopic photo of the gap between the electrodes. The size of this hole is 2 microns for two reasons. The first reason is that eventually crystals will be put on top of the contacts. These crystals will be very small, only several microns wide. The second reason is because the microcavity will make for a small mode volume in the middle of the cavity, smaller than 2 microns wide. So, the beam waist

in the cavity will fit through this hole of 2 microns.

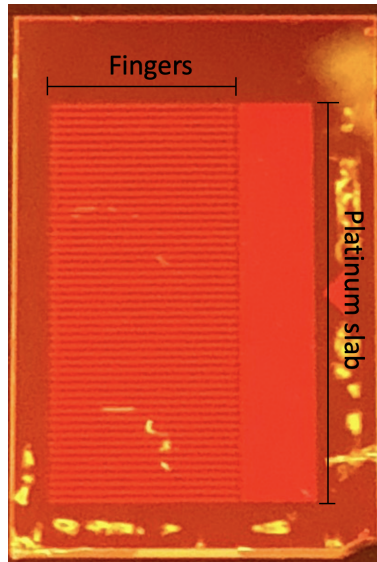


Figure 5: Image of the complete product: 11 mm x 18mm mirror with platinum contacts. On the left side of the mirror the so called platinum "fingers" and on the right side a slab of platinum. In between these areas of platinum is a 2 micron hole, see figure 6.

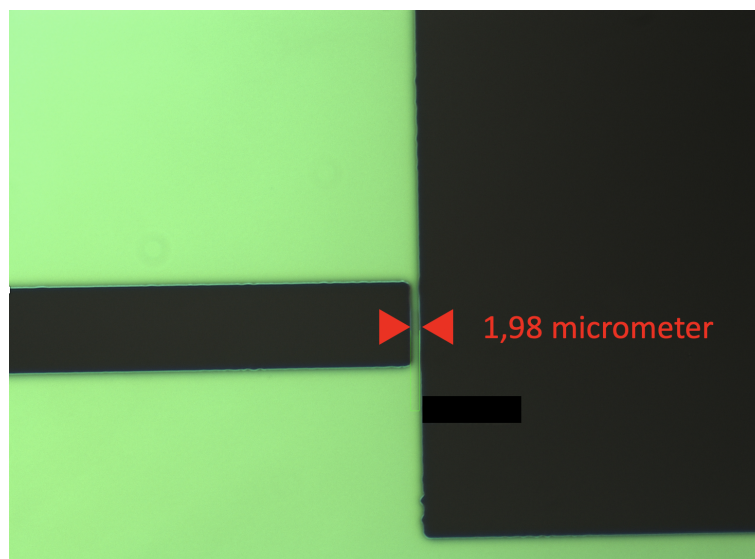


Figure 6: A hole of approximately 2 microns separates the platinum finger (left, in black) and the platinum slab (right, in black).

The contacts on top of the DBR mirror are made in several steps, each

step using different fabrication techniques. Below, the steps and corresponding techniques are explained:

- step 1: cleaning the surface of the mirror
- step 2: spincoating resist on top of the clean mirror
- step 3: patterning the resist
- step 4: evaporating metal on top of the sample
- step 5: lifting off left-over resist

step 1: cleaning the surface of the mirror

First the mirrors are cleaned using a Base Piranha [13]. Base Piranha is a mixture of ammonia solution and hydrogen peroxide in water (1:1:5). This mixture is heated to 75 °C and samples (in this case DBR mirrors) are put into the mixture for 15 minutes. After 15 minutes the samples should be rinsed with demineralized water first and 2-propanol (IPA) second. The samples can now be dried using a nitrogen gun. To keep them clean for approximately two weeks, the samples need to be stored in an oxygen-low cabinet. This cleaning method is used to get rid of all organic residue, so that there is a better adhesion and less chance of failure in the following steps. After this cleaning process the samples are ready to be covered with resist.

step 2: spincoating resist on top of the clean mirror

To create a pattern on top of the mirror, negative resist will be spincoated on top of it. After spincoating the resist, the samples will be patterned using UV-lithography. Since the resist on the samples will be patterned using a negative light-mask, the resist that will be used is also a negative resist. A negative light-mask is a mask where only the pattern of the mask is exposed to UV-light when put on top of the sample. To be able to do so, the sample is first spincoated with two types of resist.

The first type of resist is LOR (Lift-off resist) 20B diluted with cyclopentanone (1:1). This type of resist is used to create an undercut after development to make the eventual lift-off of excess metals easier. In figure 7 a schematic of how this sample eventually develops is shown. This type of resist is spincoated such that it reaches a thickness between 600-800 nm. After spincoating the sample is baked on a hotplate at 150 °C for 3 minutes, to let the solvent of the resist evaporate.

The second type of resist is S1805. S1805 is a light-sensitive resist. This property is used to develop a pattern after UV exposure. The S1805 is spincoated such that it reaches a thickness of 500-700 nm. After spincoating, it has to be baked at 115 °C for 1 minute to let solvent of the resist evaporate. A schematic of this process is shown in figure 8.

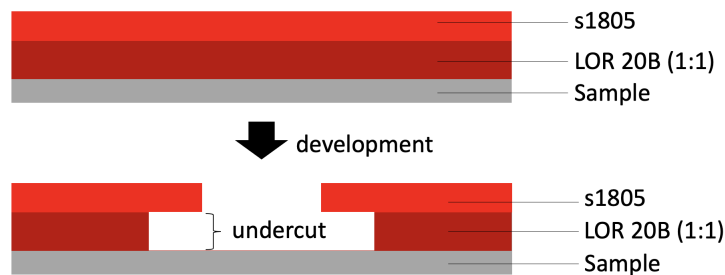


Figure 7: A side-cartoon of how the resist develops. The undercut that is created after development makes the lift-off easier.

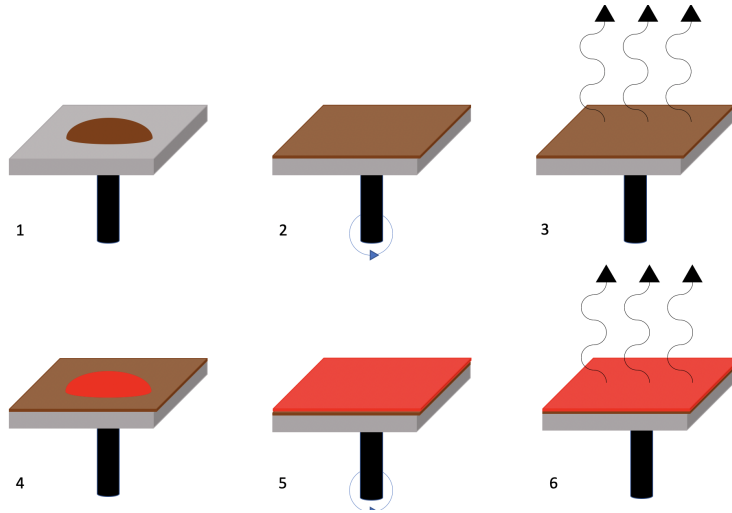


Figure 8: Spincoating resist. 1) An amount of diluted Lift-Off-Resist (LOR) 20B, 1:1, is deposited on top of the sample. 2) The sample is spun at 4000 rpm. 3) The sample is baked at 150 °C for 3 minutes. 4) An amount of S1805 resist is deposited on top of the sample. 5) The sample is spun at 4000 rpm. 6) The sample is baked on 115 °C for one minute.

step 3: patterning the resist

When the light-sensitive resist is deposited on top of the sample, the next step will be UV-lithography to make a pattern in this resist. UV lithography uses UV-light to transfer a pattern from light-mask onto resist. The pattern on the light-mask is similar to the one in figure 5, except the fingers are shorter on the light mask and have to be extended on the sample. To extend the fingers, the sample is exposed to UV-light and developed twice. First only the left part of the pattern is exposed with 25 mJ/cm² for 5 seconds. The sample can now be developed in MF-319 for 3 seconds, just to see a little bit of the pattern under the microscope so that the light-mask and the pattern can be aligned. When the fingers are visible under a microscope, the sample can be aligned with the light-mask to expose the rest of the pattern on top of the sample. Depending on the thickness of the resist, we now develop in MF-319 between 25-40 seconds (depending on the exact thickness of the resist). The sample will now look like in figure 9.

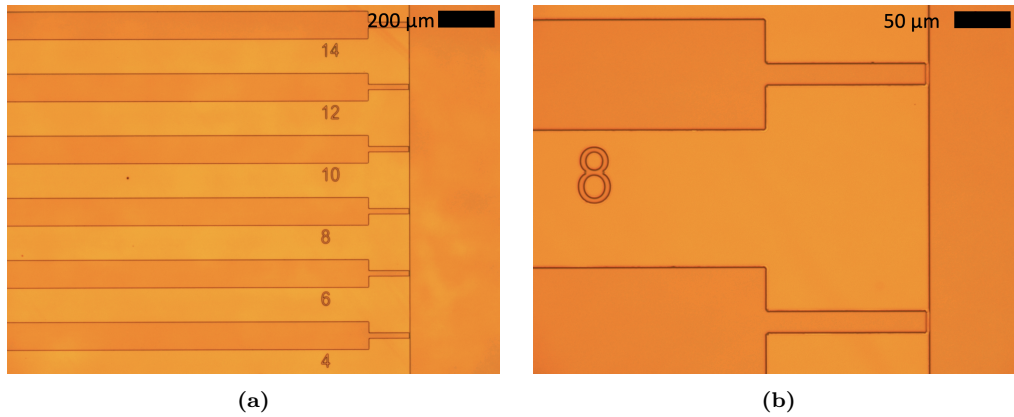


Figure 9: Top view of the patterned resist. a) A 10x magnification of the sample after development. The dark orange areas are the mirror's surface and the brighter oranges areas are areas where there's still resist left. b) A 50x magnification of the sample after development.

step 4: evaporating metal on top of the sample

Once the pattern is developed into the resist, we are able to evaporate metal on top of the sample. To evaporate metal, the sample is put into the E-flex at the Amolf Nanolab. The E-flex is an E-beam physical vapor deposition apparatus. The sample is loaded into the vacuum chamber of the E-flex where an electron beam is used to heat metals into their gaseous phase. Metals in their gaseous phase float around in the vacuum chamber until they touch the surface of the sample, forming a film of this metal on top of it. To make reliable contacts we need a film thickness with a minimum of 130 nm platinum. Platinum does not adhere to the mirror (with a glass surface) by itself, so an adhesion layer of 5 nm chromium is firstly put onto the sample. After deposition the sample looks as in figures 10a and 10b.

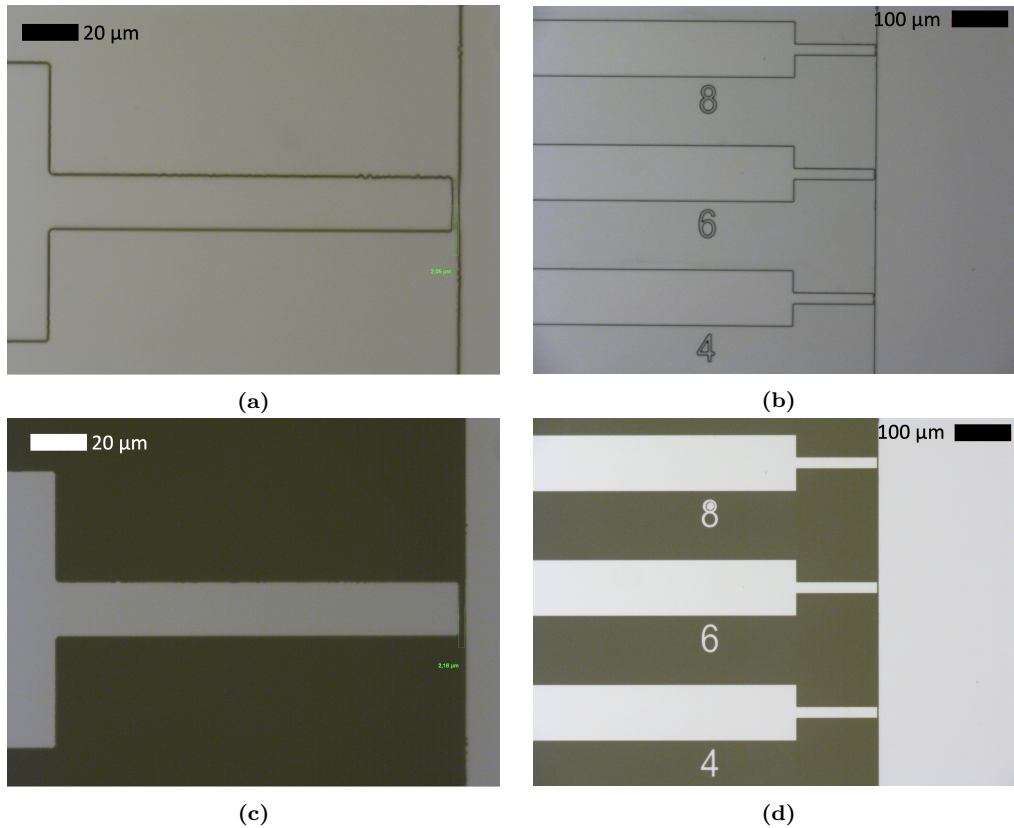


Figure 10: a) 50x magnification of the sample covered in platinum, after deposition and before lift-off. The gap between the two features is approximately 2 microns. b) 20x magnification of the sample covered in platinum, after deposition and before lift-off. c) 50x magnification of the sample after lift-off. In light-grey we can see the platinum contacts and the dark grey area is the background mirror. The gap between the two features is approximately 2 microns. d) 50x magnification of the sample after lift-off. In light-grey we can see the platinum contacts and the dark grey area is the background mirror.

step 5: lifting off left-over resist

The last step of the process, the most critical one, is lift-off. The lift-off process gets rid of all the remaining resist and thereby loses the excess metals. To get rid of all the material outside of the pattern, we put the sample into a 60 °C bath of N-methyl-2-pyrrolidone, NMP. The NMP will dissolve the left-over LOR and s1805 resists, so that the metal on top of it will let go. The only thing that remains is the pattern of the light mask in platinum on top of the mirrors, see figures 10c and 10d. These are the finished platinum

contacts on top of the mirror, see figure 5.

4 Crystal Exfoliation and Transfer

The fabricated crystals need to be exfoliated in order to reach the right thickness and lateral size. A thickness of approximately 300 nm is desired. When these crystals have the right thickness and lateral size, they have to be transferred onto the platinum electrodes to measure their conductivity. In this chapter, the process of exfoliation of the perovskite crystals and the transfer of the exfoliated crystals onto the platinum electrodes is explained. When exfoliation and transfer have been done, the setup will look similar to figure 11, minus the electrical probes.

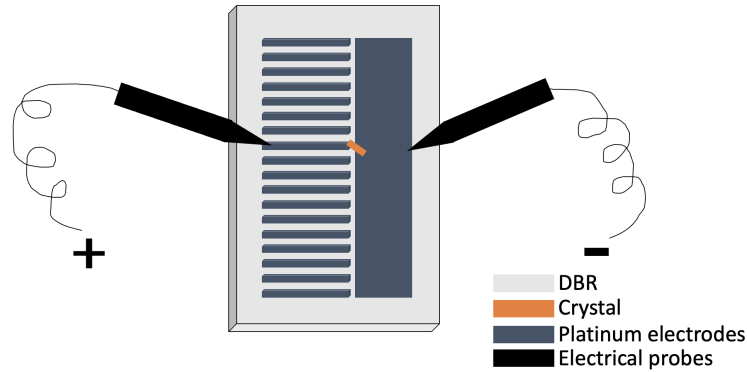


Figure 11: A schematic of the finished product and the way current will be measured. The grey sample is an 11x18 mm DBR mirror with platinum electrodes, on top of which a crystal is placed. Current through the crystal can be measured using a probe system attached to a source measurement unit.

4.1 Crystal Exfoliation

Once the crystals have successfully grown, it is time to reduce their size and thickness. Before exfoliation, the thickness can reach up to 2 mm, while the desired thickness of the crystals is approximately 300 nm. To reduce the thickness a seemingly simple method called “the scotch tape method” is used. This exfoliation method is a form of mechanical exfoliation. The principle of the scotch tape method is easy: for the first exfoliation a piece of Nitto tape (General purpose, only adheres to certain surfaces. Luckily it

adheres to the surface of the crystal.) is placed on top of the bare crystal. This tape is then peeled off leaving smaller and thinner crystals on the tape. This piece of tape, with corresponding crystals is now your first exfoliation. For the second exfoliation, the same piece of tape is covered with a second (clean) piece of tape. This second piece of tape is then peeled off again and is now the second exfoliation. This process is repeated until you reach the desired thickness for the crystals. The thickness can be measured using a profilometer, available at the Amolf facilities. In figure 12 we can see the size of the crystals for each next exfoliation.

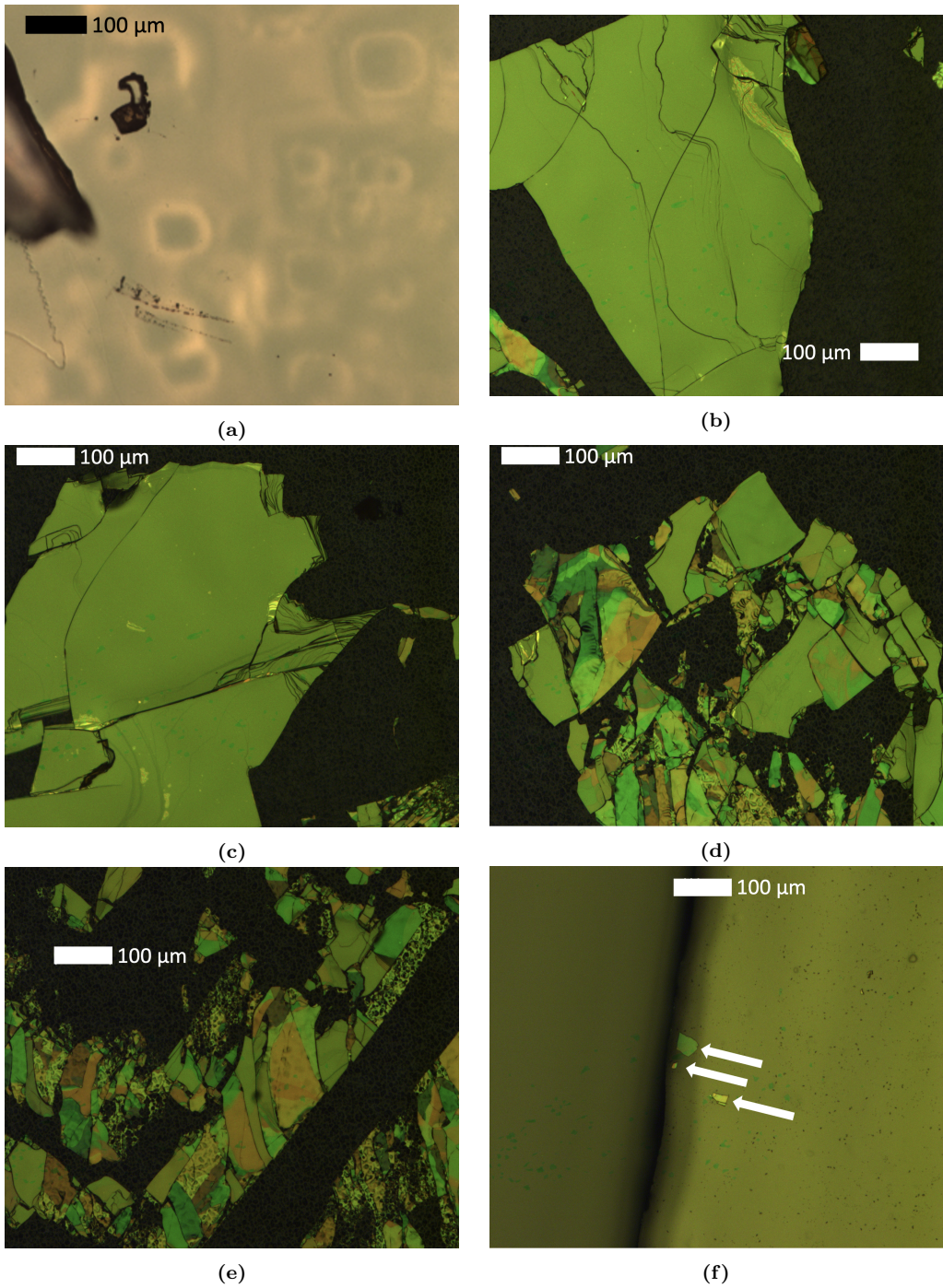


Figure 12: The scale bar in every picture is 100 micrometer a) First exfoliation. A very large area of crystal with almost no imperfections. b) Second exfoliation, reducing the size of the crystal. c) Third exfoliation. d) Fourth exfoliation. e) Fifth exfoliation. f) Three small crystals after transfer onto GEL-FILM PDMS.

4.2 Deterministic Transfer onto Electrodes

When the desired thickness of the crystals is reached, it is time to transfer the crystals from the Nitto tape onto a piece of PDMS. PDMS had viscoelastic properties which are good for transfer onto PDMS and onto electrodes. These properties make sure that when large and high velocity motions are used, crystals stick to the PDMS. At small and low velocity motions, crystals are more likely to stick to the other surface on which the PDMS is placed. For the purpose of this research the crystals are transferred onto GEL-FILM®PF-60-X4 from the company "Gel-Pak", which is an industrial form of PDMS very suitable for transfer. This type of PDMS has very little imperfections and a smooth surface.

For the transfer from Nitto tape to PDMS, the last exfoliation (on Nitto tape), with approximately 300 nm thin crystals, is placed on top of a piece of PDMS and quickly ripped off. The fast motion will make it more likely for the crystals to stick to the PDMS than onto the tape, leaving some crystals on the surface of the PDMS, see figure 12f.

For the deterministic transfer from PDMS onto the platinum contacts on the mirror a microscope was built, such as the one in figure 13. The microscope has two moving stages which make it possible to place micrometer sized crystals on a determined place on the contacts. In figure 13a a picture from reference [14] can be seen. On the left side of this figure, there is a stamping stage. Once the crystals have been transferred onto PDMS, the PDMS is suspended upside-down from the stamping stage. This stamping stage is able to move in all directions (x , y , z). This allows the crystal, attached to the stamping stage, to be moved around while it is suspended above the patterned mirror. The mirror is placed on the sample stage of the microscope, which can also be seen through the microscope.

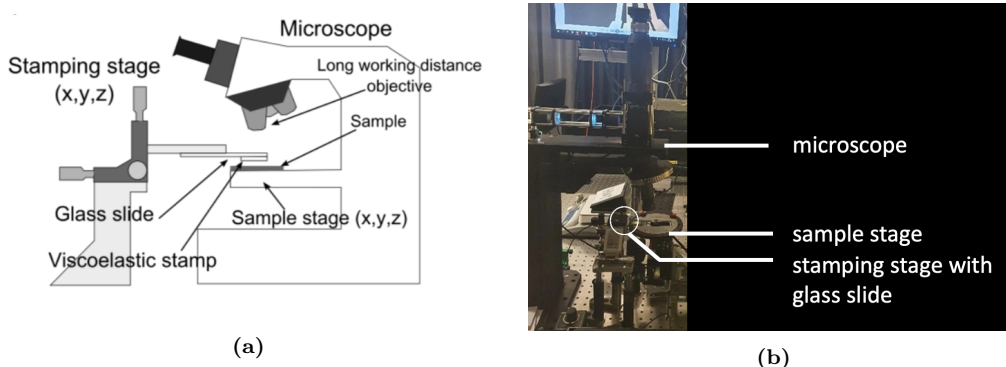


Figure 13: Figures of the microscope used for the deterministic transfer of perovskite crystals onto electrodes. a) figure from reference [14], where the microscope set-up can be seen schematically. b) a photo of the microscope set-up as used in the lab, similar to the one seen on the left.

Once the crystal is suspended above the right place on the mirror, the crystal can be brought down and stamped onto the mirror. To clarify the process, microscope images can be seen in figure 14. The placement of the crystal makes use of the viscoelastic properties of the PDMS. This time, low velocity and small movements will make the crystal more likely to stick to the surface of the mirror. In figure 14a, in the yellow circle, there is a crystal that has to be placed on top of the 2 micrometer gap between the platinum electrodes (orange parts) on the mirror. A darker area on the top of the figure shows where the PDMS is already in contact with the mirror. The lighter area at the bottom of the figure is where the two surfaces are not touching yet. For a successful transfer of the crystal it is vital that the PDMS around the to-be-placed crystal is touching the surface of the mirror, i.e. preferably no air bubbles surrounding the crystal.

In figure 14b the PDMS is pushed down more and the darker area grows bigger, meaning the surfaces are touching. More importantly, as can be seen, there is no air around the to-be-placed crystal. Once the crystal is in good contact with the mirror it is time to very slowly peel off the PDMS. This is done with a piezoelectric actuator, taking care of the very slow upward motion of the stage. It is now visible in figure 14c that the touching areas

are getting smaller again, thus the surfaces are letting go of each other. To make sure that the crystal is now stuck to the mirror, the PDMS is removed from the microscope set-up. In figure 14e, the PDMS is removed and the crystal is placed at the right place on the contacts.

The complete sample, including mirror, contacts, and crystal, is now finished and ready to be inserted into the microcavity. Before that, the optical and electrical characterization of the crystals is done.

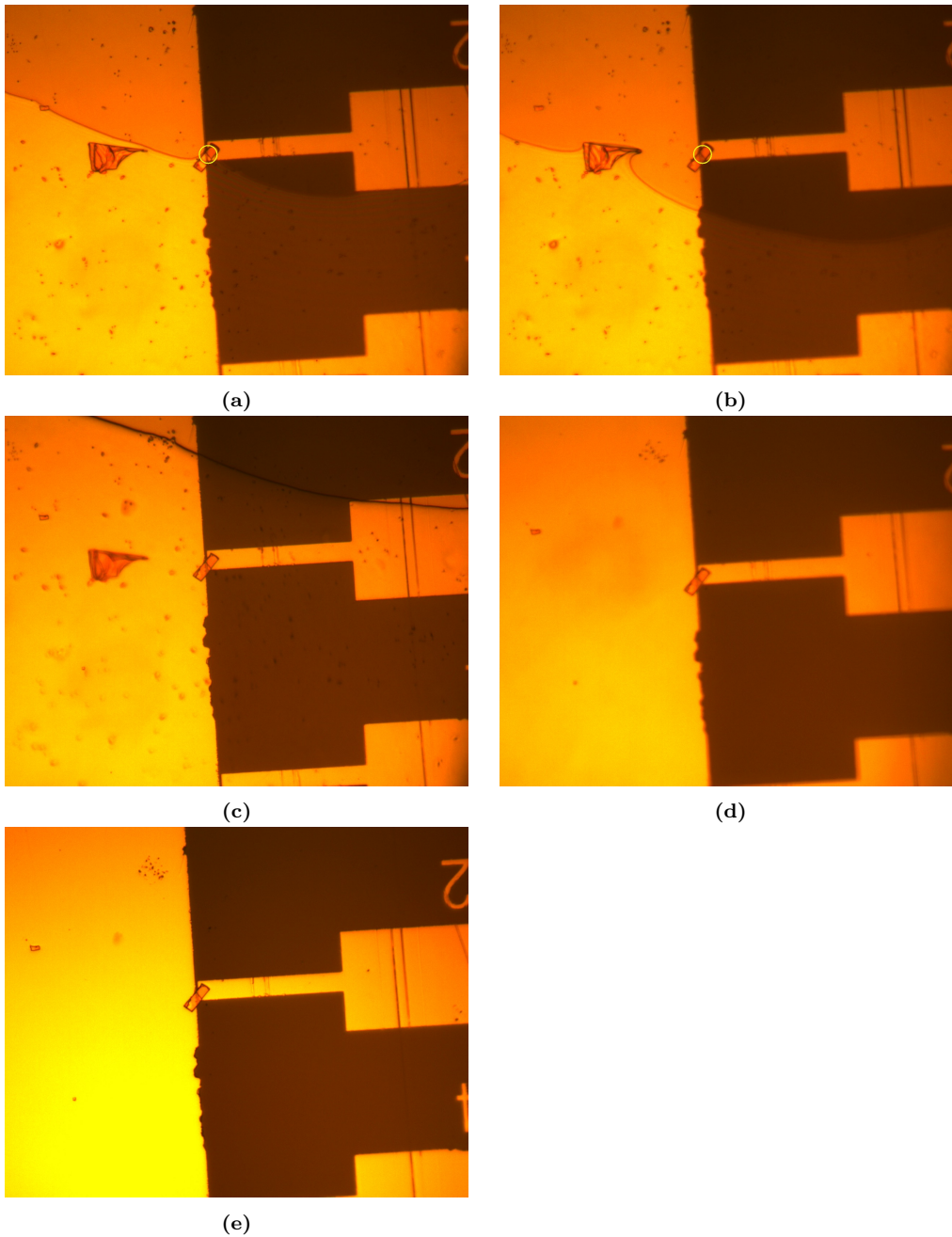


Figure 14: Transfer of a perovskite semiconductor crystal onto the gap between the electrodes on a patterned mirror. a) In the yellow circle is the to-be-placed crystal. The dark area at the top is the place where PDMS and the mirror are already touching. The lighter area at the bottom is where the PDMS and the patterned mirror are not touching yet. b) The stamping stage is pressed down and the area where the surfaces are touching is growing. The crystal is not surrounded by air bubbles, this indicates a successful transfer onto the platinum electrodes. c) The stamping stage is lifted up very slowly and the touching areas are decreasing in size again. d) The PDMS is completely removed from the setup. e) The small crystal remains at the right place on the patterned mirror, transfer successful.

5 Optical and Electrical Measurements

In this section the results of the optical and electrical characterization of the crystals is shown. The results are discussed and compared to values as seen in theory.

5.1 Optical Measurements

To optically characterize the perovskite crystals, both photoluminescence and absorbance were measured. Photoluminescence is the emission of light from the crystal after it has been excited by a laser and falls back into the ground state.

Absorbance spectroscopy is performed to show the optical absorbance of the crystal as a function of wavelength. From the absorbance spectrum we know the maximum absorbance, which is characteristic for the substance that is irradiated. From the absorbance peak we can derive the exciton energy and linewidth.

Absorbance and photoluminescence are measured to reveal whether the crystal is suitable for a strong coupling experiment. Because strong coupling requires strong excitonic absorption and a narrow linewidth in the spectrum.

In the graph below, it is shown that the photoluminescence has a peak at approximately $\lambda_{PL} = 527nm$, the absorbance peaks at approximately $\lambda_A = 517nm$. These numbers are favorable, because the DBRs used in the experiment have a maximum transmission at $\lambda = 530nm$.

The shift between the absorbance and the photoluminescence peak is corresponding to 45.2 meV, this is called the Stokes shift and shows the energy that is lost in the crystal between absorbance and emission due to relaxation or dissipation in the crystal.

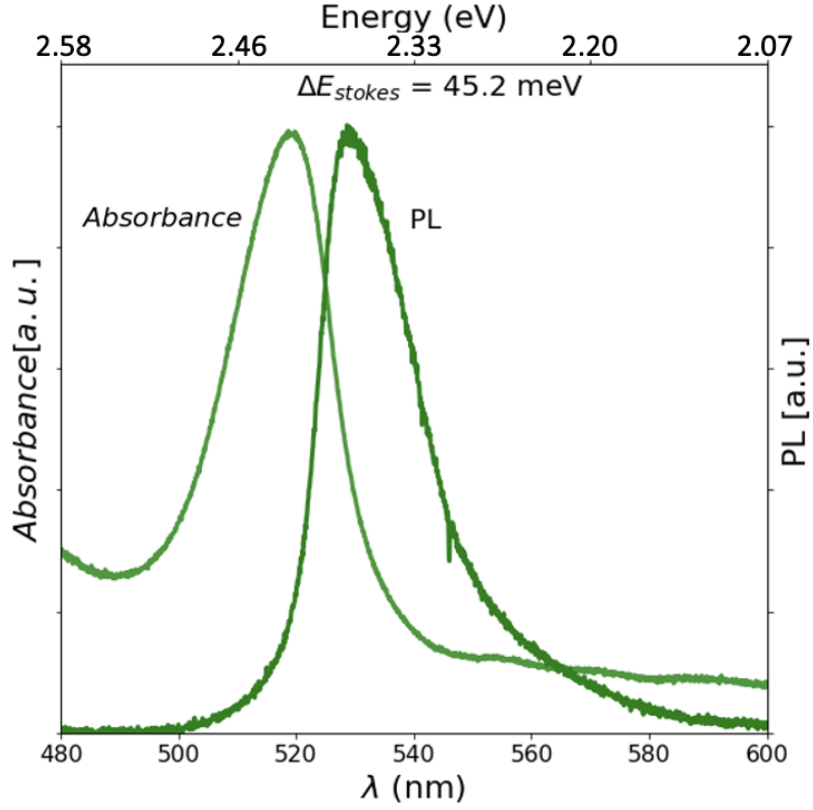


Figure 15: Absorbance and photoluminescence for $2(PEA)PbI_4$ in bulk. Peaks for absorbance and photoluminescence are at $\lambda_A = 517$ and $\lambda_{PL} = 527$ respectively. Stokes energy is corresponding to 45.2 meV.

The values that were found for the PL peak and the absorbance peak correspond to the values found in similar studies in references [15], [16], and [17]. In figure 15, it can be seen that the PL and the absorbance peak of these crystals are dominated by an exciton band at roughly 2.4 eV, consistent with a large exciton binding energy [18]. Materials having a large binding energy are specifically interesting for optoelectronics and therefore very suitable for the purpose of this research.

5.2 Electrical Measurement

In order to electrically characterize the perovskite crystals a setup like in figure 16 was made. In this setup, a crystal was transferred onto a contacted mirror. Two electrical probes were attached to both sides of the platinum electrodes, so that current is able to flow through the crystal. These probes are connected to a Source Measure Unit (SMU) that is able to precisely measure the current and voltage at the same time. The SMU is connected to a computer where all data is received and processed.

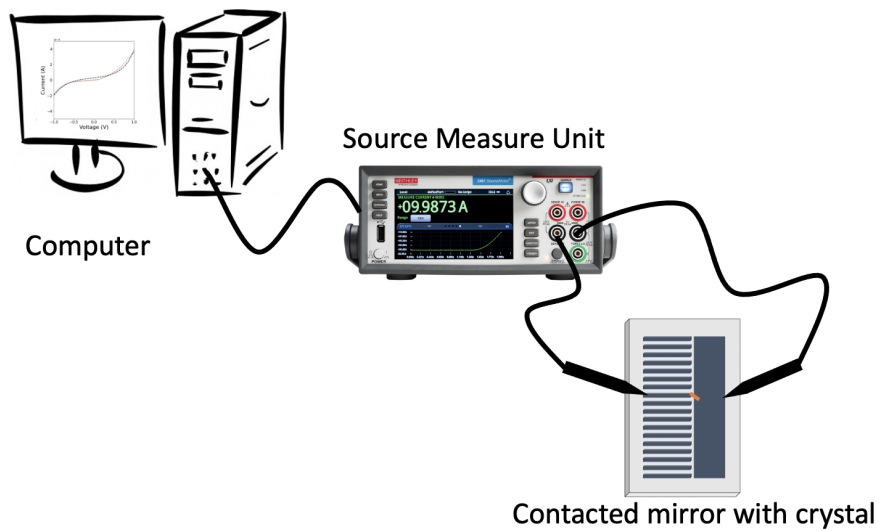


Figure 16

In figure 17, several IV curves from electrical measurements made on the perovskite crystals can be seen. These IV-curves were fitted using the Simmons model [19]. The Simmons model is a way to describe the electron transfer through these crystals. It can be used to approximate the barrier widths, L , and the barrier heights, ϕ_0 of the crystal.

This Simmons model [20] gives current density, i , as:

$$i = \frac{e^2}{2\pi h L^2} \left\{ \left(\phi_0 - \frac{V}{2} \right) \exp \left[-K \sqrt{\phi_0 - \frac{V}{2}} \right] - \left(\phi_0 + \frac{V}{2} \right) \exp \left[-K \sqrt{\phi_0 + \frac{V}{2}} \right] \right\} \quad (1)$$

where:

$$K = \frac{4\pi L}{h} \sqrt{2me}. \quad (2)$$

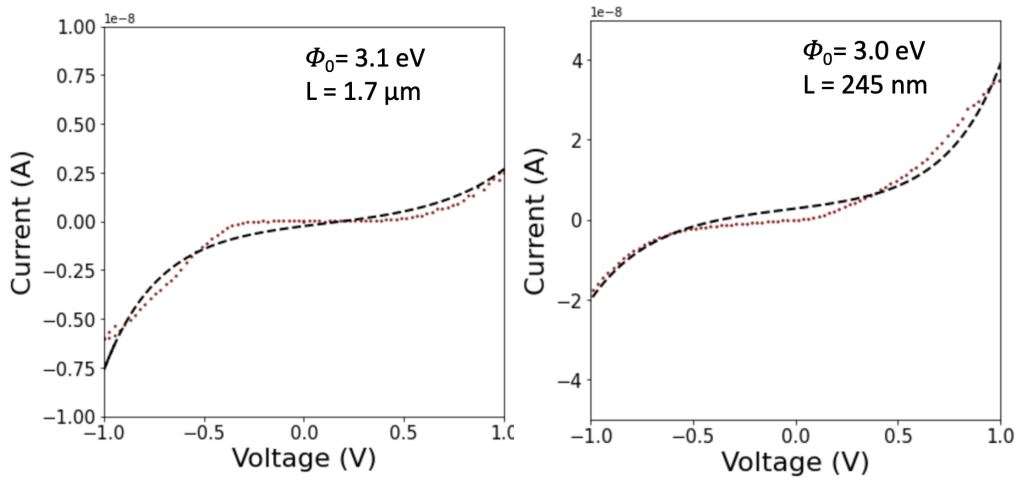
- i = current density
- ϕ_0 = mean barrier height
- L = barrier length
- e = electron charge
- m = electron mass
- h = Planck's constant
- V = voltage

With this approximation to the IV-curve, it is possible to get values for the mean barrier height, ϕ_0 , and the barrier length, L [20]. The barrier height is the difference between the metal work function and the electron affinity of the semiconductor. It is dependent on the combination of the semiconductor and the metal that is used (0.5–1 eV, for Si). Typical Schottky barrier heights that were found in platinum-semiconductor contacts are between the values of 0.4 - 0.9 eV [21] [22] [23].

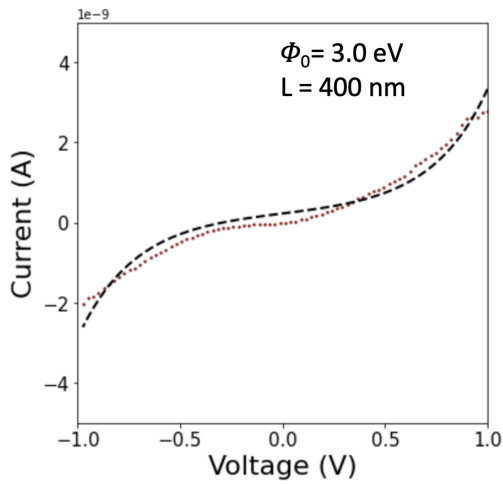
The barrier width is dependent on, among other things, the doping density of the semiconductor (the concentration of carriers in this semiconductor). It is therefore possible to tune barrier widths in order to allow more or fewer electrons [24]. Typically the size of the barrier width is on the order of $L = 10 - 1000$ nm [25].

Figure 17 shows measurements to crystals and their values for ϕ_0 and L and corresponding IV-curves. In figures 17a, 17b and 17c, we can see IV measurements on the perovskite crystals. All these figures were measured from -1 V to 1 V. Note that the scale-bars are different. In figures 17a and 17b the current is on the order of $10^{-8}A$ and in figure 17c it is on the order of $10^{-9}A$. The barrier heights for all these crystals is simulated with the Simmons model and is either 3 eV or 3.1 eV. The barrier width however, is not consistent and is $1.7 \mu m$ in figure 17a, 245 nm in figure 17b, and 400 nm in figure 17c. All these graphs show a non-ohmic contact (no linear IV-curve), as can be expected from metal-semiconductor connections.

When comparing the barrier heights, ϕ_0 , to values found in literature, the barrier height found in these measurements is at least three times higher. Even though the barrier height is tunable and can thus for a certain degree be chosen, we are unsure of the origin of the value here reported. When comparing barrier widths, L , to that of normal values, only the barrier widths in figures 17b and 17c are of normal value. The barrier width in figure 17a is too big. And again, we are unsure of the values reported here. More importantly, the Simmons fit seems to be not a very good fit for the measured IV-curves. The uncertainty of the parameters could be large enough so that the fit parameters are comparable, but no quantitative estimates of the uncertainty is given. The parameters should therefore be taken with a grain of salt.



(a) The red dots correspond to the IV-measurement and the black stripes to the Simmons fit. The current was measured from -1 to 1 V and the vertical axis is on the order of $10^{-8}A$. (b) The red dots correspond to the IV-measurement and the black stripes to the Simmons fit. The current was measured from -1 to 1 V and the vertical axis is on the order of $10^{-8}A$.



(c) The red dots correspond to the IV-measurement and the black stripes to the Simmons fit. The current was measured from -1 to 1 V and the vertical axis is on the order of $10^{-9}A$.

Figure 17: IV-curves of 3 different crystals, with corresponding barrier heights, ϕ_0 , and barrier lengths, L . Notice the different scales for the different graphs. Red dots correspond to the actual measurement and the black stripes to the Simmons fit.

6 Conclusion and Outlook

In this chapter, the results of this thesis are repeated. Furthermore, it explains what has been done and also what should be done next.

The electrical measurements on the bare perovskite crystals did not show a consistent result. Not only did it not show a consistent result, we are unsure of the values that are reported here. This could be due to the fact that the method of measuring is not accurate enough. This electrical measurement is a highly sensitive measurement, since we are dealing with exceptionally small and thin crystals and a low current. Therefore, the process of measuring the current through the crystals should be altered in order to measure more exact. In order to do so, there should be electrical wires attached to every finger of the contacts on the DBR mirror. These wires will make a more steady connection between the contacts and the SMU.

The optical results of the crystals show great promise for the crystals to be put into a microcavity and measuring its enhanced current due to strong coupling and exciton-polaritonic effects. The photoluminescence has a peak at 527 nm and the absorbance at 517 nm. These two values were compared to similar studies and it was found that they are comparable. The PL and the absorbance peak of these crystals are dominated by an exciton band at roughly 2.4 eV, consistent with a large exciton binding energy [18]. Materials having a large excitonic binding energy are specifically interesting in optoelectronics and therefore very suitable for the purpose of further research.

In this thesis the ground work for this further research was done. This ground work encompassed:

- **Fabrication:** The perovskite semiconductor crystals that were used in this research had to be grown and to eventually measure the conductivity of these crystals, platinum electrodes were made on top of high reflectivity mirrors.
- **Exfoliation and Transfer:** The perovskite crystals had to be exfoli-

ated until right size and thickness, after which they had to be transferred onto the platinum electrodes.

- **Optical and Electrical Characterization:** The bare perovskite crystals had to be characterised both optically and electrically.

The next step in this research is altering the way that current is measured so that it matches the very sensitive measurement. When this is achieved, the crystals are ready to be put inside the microcavity and have their current measured during excitation of a laser. Hopefully, this thesis will be helpful in accomplishing the final goal of the research: to modify the conductivity of a perovskite semiconductor by strongly coupling electronic excitations in these semiconductors to cavity modes.

References

- ¹D. Hagenmüller et al., “Cavity-enhanced transport of charge”, *Phys. Rev. Lett.* **119**, 223601 (2017) 10.1103/PhysRevLett.119.223601.
- ²D. Hagenmüller et al., “Cavity-assisted mesoscopic transport of fermions: coherent and dissipative dynamics”, *Phys. Rev. B* **97**, 205303 (2018) 10.1103/PhysRevB.97.205303.
- ³E. Orgiu et al., “Conductivity in organic semiconductors hybridized with the vacuum field”, *Nature Materials* **14**, 1123–1129 (2015) 10.1038/nmat4392.
- ⁴F. Ledee et al., “Fast growth of monocrystalline thin films of 2D layered hybrid perovskite”, *CrystEngComm* **19**, 2598–2602 (2017).
- ⁵Y. Deng Haug, “Exciton-polariton Bose-Einstein condensation”, *Rev. Mod. Phys.* **82**, 1491–1495 (2010) 10.1103/RevModPhys.82.1489.
- ⁶L. Novotny, “Strong coupling, energy splitting, and level crossings: a classical perspective”, *American Journal of Physics* **78**, 1199–1202 (2010) 10.1119/1.3471177.
- ⁷J. K. D Snoke, “The new era of polariton condensates”, *Physics Today* **70**, 54–60 (2017) 10.1063/pt.3.3729.
- ⁸H. Chen et al., “1.14 - nonlinear nanophotonics with 2D transition metal dichalcogenides”, in *Comprehensive nanoscience and nanotechnology (second edition)*, edited by D. L. Andrews et al., Second Edition (Academic Press, Oxford, 2019), pp. 305–318, <https://doi.org/10.1016/B978-0-12-803581-8.11340-2>.
- ⁹J. K. Asane et al., “Study of electrical conductivity of the poly(3 hexylthiophene-2, 5-diyl) polymer in resonant Fabry–Perot cavities”, *Journal of Nanophotonics* **13**, 1–6 (2019) 10.1117/1.JNP.13.026007.
- ¹⁰E. S. H. Kang et al., “Charge transport in phthalocyanine thin-film transistors coupled with fabry–perot cavities”, *J. Mater. Chem. C* **9**, 2368–2374 (2021) 10.1039/D0TC05418F.

- ¹¹T. Fujita et al., “Tunable polariton absorption of distributed feedback microcavities at room temperature”, English, *Physical Review B - Condensed Matter and Materials Physics* **57**, 12428–12434 (1998) 10.1103/PhysRevB.57.12428.
- ¹²G. Lanty et al., “UV polaritonic emission from a perovskite-based microcavity”, *Applied Physics Letters* **93**, 081101 (2008) 10.1063/1.2971206.
- ¹³*Base piranha recipe*, https://amolf.nl/wp-content/uploads/2016/09/process_data_base_piranha.pdf, Accessed: 2021-08-31.
- ¹⁴A. Castellanos-Gomez et al., “Deterministic transfer of two-dimensional materials by all-dry viscoelastic stamping”, *2D Materials* **1**, 011002 (2014) 10.1088/2053-1583/1/1/011002.
- ¹⁵Zhang et al., “Excitonic properties of chemically synthesized 2D organic–inorganic hybrid perovskite nanosheets”, *Advanced Materials* (2018) 10.1002/adma.201704055.
- ¹⁶Zhang et al., “Controlled aqueous synthesis of 2D hybrid perovskites with bright room-temperature long-lived luminescence”, *J. Phys. Chem. Lett.* (2019) 10.1021/acs.jpcllett.9b00934.
- ¹⁷Z. et al., “Giant Rashba splitting in 2D organic-inorganic halide perovskites measured by transient spectroscopies”, *science advances* (2017) 10.1126/sciadv.1700704.
- ¹⁸X. Hong et al., “Dielectric confinement effect on excitons in PbI_4 -based layered semiconductors”, *Phys. Rev. B* **45**, 6961–6964 (1992) 10.1103/PhysRevB.45.6961.
- ¹⁹J. G. Simmons, “Generalized formula for the electric tunnel effect between similar electrodes separated by a thin insulating film”, *Journal of Applied Physics* **34**, 1793–1803 (1963) 10.1063/1.1702682.

- ²⁰D. Axford et al., “Molecularly resolved protein electromechanical properties”, *The Journal of Physical Chemistry B* **111**, PMID: 17628094, 9062–9068 (2007) [10.1021/jp070262o](https://doi.org/10.1021/jp070262o).
- ²¹S. Kwon et al., “Probing the nanoscale Schottky barrier of metal/semiconductor interfaces of Pt/CdSe/Pt nanodumbbells by conductive-probe atomic force microscopy”, *Nanoscale* **7**, 12297–12301 (2015) [10.1039/C5NR02285A](https://doi.org/10.1039/C5NR02285A).
- ²²A. Shetty et al., “Temperature dependent electrical characterisation of Pt/HfO₂/n-GaN metal-insulator-semiconductor (MIS) Schottky diodes”, *AIP Advances* **5**, 097103 (2015) [10.1063/1.4930199](https://doi.org/10.1063/1.4930199).
- ²³M. et al., “Summary of Schottky barrier height data on epitaxially grown n- and p-GaAs”, Elsevier, *Thin Solid Films* **325**, 181–186 (1998).
- ²⁴D. Leadley, *Schottky barrier*, (2010) <https://warwick.ac.uk/fac/sci/physics/current/postgraduate/regs/mpagswarwick/ex5/devices/junctions/schottky/>.
- ²⁵V. V. Zhirnov and R. K. Cavin, “Chapter 2 - basic physics of ICT”, in *Microsystems for bioelectronics (second edition)*, edited by V. V. Zhirnov and R. K. Cavin, Second Edition, Micro and Nano Technologies (William Andrew Publishing, Oxford, 2015), pp. 19–49, <https://doi.org/10.1016/B978-0-323-31302-5.00002-8>.